Global Coupled EM-Electrical-Thermal Simulation and Experimental Validation for a Spatial Power Combining MMIC Array

W. Batty$^{\times\$}$, C. E. Christoffersen^{+}, A. B. Yakovlev$^{\circ}$, J. F. Whitaker$^{\#}$,
A. Mortazawi$^{\#}$, A. Al-Zayed*, M. Ozkar*, S. Ortiz*, R. Reano$^{\#}$, K. Yang$^{\#}$,
L. P. B. Katehi$^{\%}$, C. M. Snowden$^{\times}$ and M. B. Steer*

$^{\times}$Institute of Microwaves and Photonics, School of Electronic and Electrical Engineering,
University of Leeds, Leeds LS2 9JT, UK.
$^{+}$Department of Electrical Engineering, Lakehead University, 955 Oliver Road, Thunder Bay,
Ontario P7B 5E1, Canada.
$^{\circ}$Department of Electrical Engineering, The University of Mississippi, MS 38677-1848, USA.
$^{\#}$Center for Ultrafast Optical Science and Radiation Laboratory, Department of Electrical
Engineering and Computer Science, University of Michigan, Ann Arbor, MI, USA.
*Department of Electrical and Computer Engineering, North Carolina State University,
Raleigh, NC 27695-7914, USA.
$^{\%}$Schools of Engineering, Purdue University, West Lafayette, Indiana 47907, USA.
$^{\$}$Corresponding author: tel. +44 113 3432089   fax +44 113 2449451   e-mail
w.batty@elec-eng.leeds.ac.uk

Keywords: global modeling and simulation; microwave circuits; power devices; electrothermal effects; thermal modeling; thermal measurements; electromagnetic modeling; electromagnetic measurements; spatial power combiners; quasi-optical power combining.

Abstract— **A unique electromagnetic-electro-thermal global simulation tool based on a universal error concept is presented. The advantages of this electro-thermal model are illustrated by comparison with a commercial electro-thermal circuit simulator. The first description of a fully physical, electro-thermal, microwave circuit simulation, based on coupling of the Leeds Physical Model of MESFETs and HEMTs, to a microwave circuit simulator, fREEDA^{TM} (NCSU), is presented. The modeling effort is supported by parallel developments in electro-optic and thermal measurement. The first fully coupled EM-electro-thermal global simulation of a large microwave subsystem, here a whole spatial power combining MMIC array, is described. The simulation is partially validated by measurements of MMIC array temperature rise, and temperature dependent S-parameters. Electro-thermal issues for spatial power combiner operation and modeling are discussed. The CAD tools and experimental characterization described, provide a unique capability for the design of quasi-optical systems and for the exploration of the fundamental physics of spatial power combining devices.**

I. Introduction

Spatial power combining and quasi-optic arrays are being developed as high power sources at millimeter wavelengths. Major advances in performance have been based largely on intuitive and empirical construction, and not obtained as the result of intensive computer aided design (CAD). Until now, no CAD tool has been able to handle the complex nature and computational magnitude of the global simulation problem, required to describe spatial power combining systems in their entirety.

This paper describes the first application of such a tool to the global coupled electromagnetic (EM)-electrical-thermal simulation of a spatial power combining array, and represents the highest level of global modeling reported to date. This is combined with the description of a joint experimental program capable of validating the global model [1].

Global modeling developments implemented in the simulations described here include: (i) a universal er-

ror concept based on state variables and local reference terminal formulations, which facilitates the tight integration of disparate analyses; (ii) a thermal multiport model based on generalized network parameters for nonlinear thermal systems, giving a fully analytical and minimal, thermal impedance matrix description of arbitrarily complex systems, without the use of numerical methods and avoiding the need for all model order reduction techniques; (iii) a generalized scattering matrix formulation that enables the cascading of EM partial models, so as to integrate differing EM analyses and develop an EM model of the distributed parts of the array, as well as supporting circuit ports with total current and voltage as required for interfacing to the circuit model; and (iv) application of the global environment to a very large microwave problem demonstrating the robustness of the approach. In short, this paper presents and validates a philosophy for global modeling of very large problems which includes minimal approximations and close adherence to system physics, as well as readily achieving global convergence.

The structure of the paper is as follows. Firstly, global circuit simulation, based on the circuit simulator fREEDA^{TM} (previously Transim), is introduced. This is followed by brief description of the compact Leeds thermal impedance matrix model of 3-dimensional, nonlinear heat flow in complex systems. The resulting coupled electro-thermal capability in fREEDA^{TM} is contrasted with a commercial electro-thermal simulator. This is followed by description of the integration in fREEDA^{TM}, of the Leeds Physical Model of MESFETs and HEMTs, yielding a unique, fully physical, circuit level simulation tool. Electromagnetic precomputation, for global EM-electro-thermal system simulation is then outlined. This is followed by brief details of a parallel program of experimental developments aimed at the characterization of microwave subsystems. Experimental measurements on the 'tray/card' X-band amplifier, Fig. 1, are presented, and compared against thermal simulations. The first global EM-electro-thermal simulation of an entire spatial power combining array is described. Finally, electro-thermal issues for spatial power combiner operation and modeling, are discussed briefly, and conclusions are drawn.

II. Global Circuit Simulation

The power combiner simulated in this study is an X-band 'tray/card' structure introduced in [2], and illustrated schematically in Fig. 1. The actual structure modeled and measured is a 5×5 MMIC array in an aluminum tray framework of size 12 cm $\times$ 9 cm $\times$ 5 cm.

Explicitly coupled global EM-electro-thermal circuit level simulation is achieved by employing the microwave circuit simulator fREEDA^{TM} [3]. fREEDA^{TM} implements a global simulation approach in which concurrent EM, circuit, mechanical and thermal analyses are supported. The high-level circuit abstraction is retained, and the results of EM and thermal analyses of the spatially distributed physical subdomains are incorporated into the circuit framework as EM network parameters and generalized thermal network parameters, respectively. This global circuit simulation philosophy is described in [4].

fREEDA^{TM} employs a local reference terminal concept [5]. The conventional nodal specification allows circuit elements to be connected in any possible combination and only one reference terminal (commonly called ground) is used. With spatially distributed circuits it is possible to make non-physical connections such as connecting a non-spatially distributed element, say a resistor, across two physically separated (relative to the wavelength) parts of the circuit, e.g., the opposite ends of a transmission line. The local reference concept avoids this kind of problem because a different reference terminal is used in each different physical location or domain. Then, in an electrothermal simulation, the thermal ground is not the same terminal as the electrical ground. This concept is therefore fundamental to the analysis of spatially distributed circuits as well as for simultaneous thermal-electrical simulations.

In fREEDA^{TM}, parameterized models [6] are used to allow the modeling of nonlinear devices in different analysis types, DC, AC, state variable harmonic balance (HB) [7], convolution transient [8], wavelet transient [9], and time-marching transient [10], using a single implementation of the device equations [3]. The state variables are not required to be artificial voltage-like or current-like quantities. In this way the number of nonlinear state variables is reduced to the minimum necessary, the models can be formulated to avoid positive exponential dependencies, and the resulting code can be developed faster and maintained more easily as the equations need only be coded once.

The use of state variables, with network parameters for distributed systems, and combined with a universal error concept, means that fREEDA^{TM} can implement virtually any physical description in its modeling scheme, with the number of nonlinear unknowns generally much smaller than the number of unknowns in

conventional circuit analysis.

fREEDA^{TM} is free software distributed under the Gnu license and is available at [11].

A. Universal error concept

The combination of state variables and the local reference terminal concept enable a global error formulation central to the CAD environment described here. First the quantities of each type of analysis (thermal circuit *etc.*) are designated as either a flux or a potential, both of which are functions of state variables. Thus when the model of a single elemental component is evaluated, one or more flux and potentials are calculated as a function of one or more state variables. For elements that are connected together, fluxes at the common terminal must sum to zero and all potentials at the common terminal must be the same. Deviations form the error which is minimized by adjusting the state variables. For example, in a circuit the flux is current, the potential is voltage, and the local reference terminals are local ground; in a thermal system flux is heat flow, the potential is temperature, and the local reference terminal is absolute zero Kelvin; in a mechanical system the flux is force, potential is position, and the local reference terminal is an inertial reference frame, *etc.* Similar interpretations can be developed for other physical systems. One of the consequences of the error formulation described here is that nonlinear solution is robust and the state variables enable problem formulation with a minimal number of unknowns and error functions. This concept, presented in this paper for the first time, is the glue that enables fully physical system level simulations integrating the disparate analyzes presented here.

III. THERMAL IMPEDANCE MATRIX MODEL

The fully analytical thermal impedance matrix model for the treatment of the global electro-thermal modeling problem, is now described briefly [12]–[14]. The Leeds thermal impedance matrix model has been described at length in [14]. This compact model is obtained through fully analytic solution of the heat diffusion equation in complex structures, based on domain decomposition into regular subvolumes. The nonlinear heat diffusion equation is converted into a fully linear equation by appropriate transformations of variable [15]–[17]. Analytic series solutions for thermal subsystems are accelerated for rapid precomputation prior to coupled electro-thermal co-simulation [18]. The thermal model is coupled to both a fully physical device simulator, the quasi-2-dimensional Leeds Physical Model of MESFETs and HEMTs [12], [13], and a circuit simulator [14]. This enables fully self-consistent electro-thermal co-simulation on CAD timescales.

The complexity of the electro-thermal simulation problem for large microwave subsystems is illustrated in Fig. 2 [19]. The aim is to provide a thermal description from sub-micron active device channels, to the $\sim$10 cm $\times$ $\sim$10 cm scale of the whole grid array, including the effects of all structure from power FET surface metallization, air bridges and vias, through to the $N \times N$ array of substrate mounted GaAs die. This thermal description must be compatible with coupled electro-thermal co-simulation of the whole device on CAD timescales.

Under successive Kirchhoff transformation of temperature, $T \rightarrow \theta$, and transformation of time, $t \rightarrow \tau$ [15]–[17], the nonlinear, 3-dimensional heat diffusion equation,

$$\nabla . \left[\kappa(T) \nabla T \right] + g(x,y,z,t) = \rho C \frac{\partial T}{\partial t}, \qquad (1)$$

becomes,

$$\nabla^2 \theta + \frac{g}{\kappa_S} = \frac{1}{k_S} \frac{\partial \theta}{\partial \tau}, \qquad (2)$$

where $\kappa(T)$ is temperature dependent thermal conductivity, $g(x,y,z,t)$ is rate of heat generation, ρ is density and C is specific heat. $\kappa_S = \kappa(T_S)$ where T_S is the Kirchhoff transformation temperature, and diffusivity $k = \kappa/\rho C$.

Construction of the time dependent thermal solution with volume heat sources/sinks and arbitrary initial conditions, requires the solution of Helmholtz's equation in Laplace transform s-space. Multi-layer systems, Fig. 3, are treated fully analytically by use of a 2×2 transfer matrix approach. Arbitrary N-level structures can be treated [14], [20]. The most general analytical subvolume solution is constructed for the generic thermal multilayer of Fig. 3.

By averaging the resulting analytical solution over power dissipating and temperature sensitive volumes and areas, the solution reduces to the thermal impedance matrix form,

$$\overline{\Delta \theta_i} = \sum_j R_{TH_{ij}}(s) \overline{P_j}, \qquad (3)$$

where $\overline{\Delta \theta_i}$ is the Laplace transformed temperature rise of element i above its initial temperature, $R_{TH_{ij}}(s)$ is the thermal impedance matrix in Laplace s-space and the $\overline{P_j}$ are the transformed time-dependent fluxes due to power dissipation in elements, $j = 1, ..., i, ...M$.

For illustration, the corresponding form of the thermal impedance matrix for a single layer is,

$$R_{TH_{ij}}(s) = \frac{1}{\kappa_S LW} \sum_{mn} \frac{I^i_{mn} I^j_{mn}}{I^i_{00}} \frac{-4}{(1+\delta_{m0})(1+\delta_{n0})} \frac{1}{\gamma^2_{mn}}$$

$$\times \begin{bmatrix} \frac{\sinh \gamma_{mn} z_{i2} - \sinh \gamma_{mn} z_{i1}}{\gamma_{mn}(z_{i2}-z_{i1})} \times \\ \frac{[\cosh \gamma_{mn}(D-z_{i1}) - \cosh \gamma_{mn}(D-z_{i2})]}{\cosh \gamma_{mn} D} \\ +1 - \frac{\sinh \gamma_{mn}(z_{i2}-z_{i1})}{\gamma_{mn}(z_{i2}-z_{i1})} \end{bmatrix}. (4)$$

Here, z_{i1}, z_{i2} are the z-coordinates of the planes bounding heat dissipating volume, i, in the z-direction. D_i is the corresponding $x-y$ cross-section, and

$$\gamma^2_{mn} = \left(\frac{m\pi}{L}\right)^2 + \left(\frac{n\pi}{W}\right)^2 + \frac{s}{k_S}, \qquad (5)$$

$$I^i_{mn} = \iint_{D_i} \cos\left(\frac{m\pi x}{L}\right) \cos\left(\frac{n\pi y}{W}\right) dxdy, \qquad (6)$$

with $m, n = 0, 1, 2, ...$ $R_{TH_{ij}}(s)$ then represents the generalized multiport thermal Z-parameters for a thermal N-port, Fig. 3 (inset). The Z-parameters are evaluated either directly in frequency space, $s \rightarrow j\omega$, giving the impulse response, $R_{TH_{ij}}(j\omega)$, for use in harmonic balance simulation, or by analytical or numerical Laplace inversion [21], [22] in the time-domain, giving the step response, $R_{TH_{ij}}(\tau) = \mathcal{L}^{-1}\{R_{TH_{ij}}(s)\frac{1}{s}\}$, for use in transient simulation [14].

By netlist combination of such thermal subvolume solutions, with arbitrary time dependent fluxes imposed analytically at interfaces, this approach readily includes MMIC structural detail such as surface metallization, vias and air bridges, as well as global structure at the level of the whole spatial power combiner array [14].

A. Implementation and characteristics

With the above analysis the nonlinear thermal modeling problem has been rendered as a linear matrix problem. Implementation of the thermal model leads to a library of thermal elements that are handled using conventional linear modified nodal admittance matrix techniques. The nonlinear problem thus becomes one of handling the interface of thermal subvolumes with each other and electric elements, and handling nonlinear thermal radiation and convection.

The basic thermal element is a rectangular volume or multilayer and the methodology can be applied to other regular volumes such as cylinders. The method requires no volumetric or full surface discretization. Only discretization at interfaces between subvolumes is required and is used to establish interface terminals. The thermal impedance matrix approach in fREEDA^{TM} solves the 3-dimensional (3-d) heat diffusion equation exactly analytically in all its finite rectangular subvolumes, i.e. with no 1-dimensional (1-d) approximations or edge effects.

The authors have compared previously the Leeds thermal impedance matrix model against the comprehensive electro-thermal modeling and measurement capability of Szekely *et al.* [23]–[25], and the Leeds model has been clearly placed in the context of wider thermal and electro-thermal modeling in [14]. In this paper, its advantages are illustrated by comparison [19] against a state-of-the-art alternative electro-thermal modeling technology as described by Hefner and Blackburn [26], [27] (and implemented in the commercial program Saber). Here the 3-d heat flows are approximated by assuming symmetry (rectangular, cylindrical or spherical) and so reducing the corresponding 3-d heat diffusion equation to a 1-d form. An approach of *ad hoc* modifications is used to treat effects due to lateral and spherical heat spreading and the effects of 3-d geometry at edges and corners. The reduced 1-d equation is solved only approximately based on finite difference discretization. Each thermal element (*e.g.*, Si chip, package, module and heatsink) requires customized thermal analysis before entry into a component library.

In contrast, the most primitive thermal subelements in the present work are simple rectangular subvolumes and multilayers, which can be connected together at will, by netlist specification, to describe any arbitrarily complex 3-d structure. The user does not need to do any heatflow analysis in fREEDA^{TM}, this is done essentially exactly by the thermal impedance matrix approach. Once a complex structure like a metallized FET, MMIC, MCM *etc.*, has been constructed, its corresponding thermal impedance matrix can be saved for later re-use, i.e. it becomes a library component.

An implicit assumption in Saber is that heat flow is vertical, *e.g.*, from top Si chip to bottom heat sink. It allows only vertical matching of its thermal components. In contrast, thermal elements in fREEDA^{TM} can be connected vertically, horizontally and embedded within each other. This give much greater flexibility for describing complex heat flows such as the fully 3-d heat flow occurring in a 'tray/card' spatial power combiner. Fully analytical 3-d solution should also give a more accurate description of mutual thermal interaction between heating elements in, *e.g.*, a module or a multi-finger device die. In addition elementary thermal subvolumes can have arbitrary distributions of volume power dissipations located anywhere in the body of the

thermal element.

A major advantage of the thermal impedance matrix model is that it can treat fine structural detail, such as surface metallization, air bridges, vias, *etc.*, that are known to be essential in accurate description of power FETs and MMICs, *e.g.*, [28]. The method can describe such detail in a minimally compact manner, based on analytical, accelerated series, solutions which remove all resolution limitations over length scales from sub-micron device channels, to ~ 10 cm and larger structures. The number of terminals is minimal as, unlike discretized methods, no redundant internal terminals are constructed and only the minimum number of terminals consistent with connection of the electrical and thermal networks are required. This minimal description is achieved whilst still incorporating full details of fine structure on CAD timescales.

Unlike any other electro-thermal modeling technique, the thermal impedance matrix approach is independent of the simulation domain, [14], and the same thermal model (same analytical formulae and code) is used in DC, small signal, transient and harmonic balance analyses. Using harmonic balance analysis, for example, which is not available in many circuit simulators, non-linear distortion, spectral regrowth (or ACPR) can be evaluated, taking fully into account electro-thermal effects on widely varying time scales that would be problematic if transient analysis were employed. Both the transient and steady-state behaviors of mixed-signal, RF and microwave circuits are of interest to a designer [29].

IV. Fully Physical Device Model

This section describes the coupling of fREEDA^{TM} (NCSU) to the Leeds Physical Model [31]–[34] of MES-FETs and HEMTs to provide a unique, fully physical, circuit level simulation tool [35]. Very few fully physical, circuit level, CAD timescale, simulations have been described in the literature previously [36], and none of these provide an EM-electro-thermal description of microwave circuits.

The Leeds Physical Model (LPM) is a thermally self-consistent model, describing MESFETs and HEMTs by means of hydrodynamic energy transport equations in the quantum well (QW) plane: continuity, momentum conservation and energy conservation. These equations are solved in the quasi-2-dimensional (quasi-2d) approximation, producing speed-ups of over $\times 1000$ compared to fully 2-dimensional hydrodynamic models, with typical simulation times of 0.005 s, suitable for CAD. De-

spite the quasi-2d approximation, device cross-section is fully described by a charge control model propagating a series of Gaussian boxes along the device channel. In the HEMT, charge control in the direction perpendicular to the QW layer is obtained by self-consistent Poisson-Schrodinger precomputation, with results stored as a look-up table. This physical, time-domain model has large-signal capability, and is fully predictive, with device performance determined entirely by input of material parameters and device geometry such as epi-layer thicknesses, doping levels and gate recess profile.

The LPM has been integrated into the DC and transient analyses of fREEDA^{TM}. State variables have been chosen appropriate to the LPM implementation: V_{DS}, V_{GS} and temperature for the DC case; and v_{gs}, i_s and temperature for the RF case. The LPM is coupled to fREEDA^{TM} through pipes, as a separate process. This allows simple integration, with no core changes to either model, and avoiding any conflicts between global variables or functions. Multi-finger transistors, and multi-transistor systems, can then be simulated efficiently by running simultaneously several instances of the LPM. This offers obvious potential for efficient parallel implementation. The interprocess communication overhead is small.

The coupled DC implementation is illustrated by electro-thermal simulation of a power HEMT. The coupled electro-thermal circuit is illustrated in Fig. 4 (which also includes an RF source appropriate to transient simulation). The HEMT is mounted on a GaAs die, which can be described, with full inclusion of die metallization, as a thermal 1-port. A multi-finger device would be described by a similar thermal N-port. Such fully physical simulation allows, for instance, exploration of DC performance under variation of device layout and geometry. Such an analysis has been described by the authors in [37], which studies optimization of multi-finger FET design by non uniform finger spacing. Isothermal I-V curves are compared against the results of coupled electro-thermal simulation in Figs. 5 and 6.

The electro-thermal curves show the well known thermal droop characteristic of power devices. Corresponding temperature rise in the device channel, as a function of bias, is illustrated in Fig. 7.

All three figures contain 80 simulation points per curve and total simulation time was 5 minutes on a Pentium III CPU at 550 MHz. No matter what degree of detail is included in the thermal description, if nonlinear interface matching is neglected only thermal

precomputation time increases and has no impact on coupled electro-thermal simulation time.

To illustrate fully physical, self-consistent, electro-thermal transient simulation, calculations were performed describing response to turn-on of a 0.5 MHz signal (lying within the significant thermal response range of the GaAs die, which acts as a thermal low pass filter), Fig. 8.

Transient simulation over 100 cycles took 3 minutes on a Pentium III CPU at 550 MHz. Again, study of the impact of thermal factors such as die size, via placement and metallization heat capacity, neglecting interface nonlinearity, will affect only thermal precomputation time, not coupled electro-thermal simulation time.

These DC and RF simulations represent fully physical, CAD timescale, coupled electro-thermal simulation of microwave power devices and circuits. The corresponding analytical thermal description is 3-dimensional and 'nearly exact,' and the quasi-2d electrical simulation is fully physical in 3-dimensions but with neglect of any 'end effects' due to finite active device finger width.

The LPM has not yet been implemented in harmonic balance (HB) in fREEDA^{TM}. The proposed implementation of the time domain LPM will be based on the quasi-periodic Fourier transform [29] or the modified FFT approach due to Borich [30]. Highly efficient HB will require frequency domain formulation of the LPM. The time domain form of the LPM has already been implemented in 1-tone and 2-tone HB simulation by Snowden, *e.g.* [38], and the LPM has been formulated in frequency space by Xuan and Snowden [39].

The combination of the LPM with fREEDA^{TM} offers a unique capability for fully physical, coupled EM-electro-thermal simulation.

V. EM Admittance Matrix Model

The EM precomputation, required for description of a structure such as the X-band array considered here, in a global, coupled EM-electro-thermal system level analysis, is now outlined.

The EM modeling environment for the full-wave analysis of a waveguide-based aperture-coupled patch amplifier array, Fig. 1, is based on a decomposition of the entire structure into electromagnetically-coupled modules. This includes transmit and receive rectangular waveguide tapers attached to the N-port aperture-coupled patch array waveguide transitions (divider and combiner), waveguide-to-microstrip line junctions, and amplifier circuits. Each module is simulated using the most

efficient numerical technique resulting in the generalized scattering matrix (GSM) of propagating and evanescent modes. An overall response of the entire array is obtained by cascading the responses of the individual modules. Finally, the computed S-parameters are converted into Y-parameters in order to interface the EM analysis to the microwave circuit model described above.

The EM algorithm for complete modeling of the amplifier array was described in detail in [40], where all passive electromagnetic structures and amplifier networks are interfaced by cascading the GSMs of individual modules. In particular, an integral equation formulation for the induced electric and magnetic surface current density discretized via the method of moments was developed for a waveguide-to-aperture-coupled patch array, resulting in the GSM of the N-port spatial power divider/combiner. The numerical solution of a coupled system of integral equations provides an accurate characterization of all possible resonance and coupling effects in the array, including mode-to-mode coupling, mode-to-port coupling, and port-to-port coupling. An important part of this approach is the development of electric dyadic Green's functions for layered rectangular waveguides. In this formulation, dyadic Green's functions are obtained in the form of partial expansion over the complete system of eigenfunctions of the transverse (cross-sectional) Laplacian operator with the one-dimensional characteristic Green's functions in the waveguiding direction. It is clearly shown [41] that the analytical form of characteristic Green's functions for layered waveguides provides physical insight into resonance and surface wave effects occurring in overmoded layered waveguide transitions. This is related to the correlation between transverse resonances in the waveguide cross-section and surface waves propagating in a grounded dielectric slab waveguide (substrate of the aperture-coupled patch array).

The GSM for a rectangular waveguide taper approximated by double-plane stepped junctions was obtained using a mode-matching technique similar to [42]. At the double-step plane discontinuity the total field is expressed as a superposition of propagating and evanescent TE and TM modes, and the GSM for each junction is obtained by matching the total power of all modes. The overall GSM of the waveguide taper is obtained by cascading the individual GSMs of double-plane junctions.

A three-dimensional commercial finite element method program was used to model waveguide-to-

microstrip line transitions. The design criterion is based on the impedance matching of the rectangular waveguide and a microstrip line to operate with a resonance frequency of 10 GHz.

It should be noted that the GSM approach utilized here enables the cascading of EM partial modules as well as supporting circuit ports with total current and voltage as required for interfacing to the circuit model.

Thermal and EM precomputation of network parameters then allow fully coupled EM-electro-thermal global simulation on CAD timescales.

VI. COMPATIBILITY ISSUES

The distributed thermal and EM models in fREEDA^{TM} are based on generalised network parameters. The thermal description can be time or frequency domain; the EM description is purely frequency domain. In contrast, the present implementation of the LPM in fREEDA^{TM} is only time domain. This can produce compatibility issues which are now discussed briefly.

The frequency domain thermal and EM descriptions can work simultaneously with the time domain LPM in fREEDA^{TM}, but there are associated performance limitations. Currently, there does not exist in the literature a totally satisfactory solution to the time domain representation of elements defined by frequency-domain sampled data, and this problem remains a challenge. The two approaches that have been adopted in fREEDA^{TM} to attempt to solve this problem are described below.

The first approach is the convolution-based transient analysis described in [8]. A number of techniques were implemented to reduce the computational requirements of the convolution though the effect of some of these techniques on causality were not investigated. With respect to bandwidth, EM S-parameters are needed over a wide range of frequencies to obtain the impulse response with enough resolution for the transient simulation. Frequency domain treatment of the thermal system in convolution-based transient analysis is particularly problematic, due to extremely long thermal time constants, and is avoided in all convolution transient simulations by use of the time-domain thermal model. The time domain LPM can be used with the frequency domain EM model in this convolution approach, but the computational cost is high.

The second approach was the pole-zero approximation by Beyene and Schutt-Ainee [43]. The main problem here is that this method works well only up to a certain number of poles, otherwise the numerical errors in the determination of the coefficients are dominant.

As with any rational polynomial transfer function, this method by Beyene *et al.* is causal and it generates a macromodel (matrix of transfer functions) that is stable. (However, as noted in the paper by Achar and Nakhla [44], the macromodel is not guaranteed to be passive.) This method can, again, work with the time domain LPM.

The frequency domain thermal model can also be used in transient electro-thermal simulation (with the time domain LPM) using this technique, but only at the cost of thermal model order reduction from its essentially exact analytical thermal impedance matrix form (matrix of Laplace transform s-space transfer functions, $R_{TH_{ij}}(s)$).

It should also be noted that recently a new electro-thermal transient analysis has been implemented, based on direct inclusion of the time domain thermal impedance matrix (step response) in the MNAM, which allows transient electro-thermal co-simulation without requiring the near-exact analytical thermal impedance matrix model to be cast in (reduced) explicit pole-zero form. Further details will be presented elsewhere. This approach could also be used in coupled EM simulation as an alternative to the techniques described above.

As indicated in Section IV, efficient implementation of the LPM in harmonic balance simulation will require formulation of the LPM in the frequency domain (strictly giving a spectral balance description). The time domain LPM has already been used directly in HB simulation and could possibly be implemented in fREEDA^{TM} using the quasi-periodic Fourier Transform or a modified FFT approach. However, this direct time domain method will be slow due to the computational costs of repeatedly evaluating the time domain LPM response at a resolution determined by high fundamental frequencies, but over a period determined by low difference frequencies. An alternative approach might be for the LPM to be described in the time domain but using time derivative information instead of previous history for dynamic effects. This approach will be investigated.

VII. EXPERIMENTAL VALIDATION

The simulation program discussed above has been conducted jointly, and developed iteratively, with a program of experimental characterization, both EM and thermal. During the past several years, a research-prototype electro-optic (EO) near-field imaging system has been under development at the University of Michigan. The EO field-mapping technique, in which various electro-optic crystals have been utilized as both electric

field and temperature sensors, has been demonstrated to provide a thorough picture of the physical phenomena underlying the operation of a variety of microwave integrated circuits, antennas, and arrays [45], [46].

In particular, due to its spatial resolution, which has been demonstrated to be on the order of 5 μm, the EO system is very effective at isolating precisely, malfunctioning sections of a network or specific elements of a device under test during the actual operating conditions. The extremely fast response of an EO crystal to a time-varying field, along with the use of ultrashort-pulse-duration lasers to probe the effect of the electric-field on the EO crystal, has allowed the demonstration of a measurement bandwidth for the field-mapping system that exceeds 100 GHz. In addition, by utilizing the field-sensitive axes present in EO crystals, it is possible to map three vectorial field components separately. Furthermore, since all of the RF instruments in the EO measurement system have a 10-MHz common reference signal that originates with the phase-locked laser, it is possible for the EO system to obtain the amplitude and phase of the electric field simultaneously during the imaging process. Finally, a non-contact measurement configuration combined with optical-fiber-coupled, low-dielectric-constant EO crystals [47] makes the field-mapping system less intrusive to a device under test than any other near-field measurement method.

It is also possible for the EO system to map simultaneously both electric field and temperature distributions, by utilizing an optical absorption modulation that takes place at certain probe-laser wavelengths within semiconductor EO crystals. This accomplishment takes advantage of two important facts: not all of the laser light sampling the radiated electric field is coherently modulated by the high-frequency field; and the bandgap of GaAs is essentially changing linearly in a large temperature range of interest for our laser wavelength. This allows for the combined electro-thermal examination of active microwave and millimeter-wave circuits with a single probe and the ability to calibrate electric field data that is corrupted when the probe is placed in areas where temperature variations are present. The technique has been used to compare electric and thermal fields on a patch antenna radiating high-power [48], and it is now being applied to the combined electro-thermal examination of the microwave elements in the quasi-optical power-combining array described here.

A. Experimental results

Infrared thermal images of the X-band spatial power combiner have been obtained using an Inframetrics ThermaCam, Fig. 9.

Allowing for the difficulties of emissivity correction and specification of external heat flux coefficients, and uncertainties in device and material parameters, agreement between experiment and simulations is found to be reasonable, partially validating the global model.

Thermocouple measurements were also made internally and externally to the X-band array at turn-on. Supply voltage to the MMIC amplifiers was 6.001 V, and total current drawn 3.285 A, giving a DC power dissipation of 19.7 W. Fig. 10 shows measured point temperature traces at: the bottom of the third tray in the 'tray/card' power combiner stack (Tray 3); at the base of the power amplifier array (Base); and on top of the array (Top). The lowest trace represents room temperature (Room). As expected, the bottom of tray 3, at the center of the aluminum framework, is at the highest temperature. The temperature variation across the array is less than 5 K at the maximum measured temperature rise of 27 K (after 35 minutes). The vertical dashed line is at t = 2110 s at which time the power was turned off. Prior to turn-off, temperature is seen to be rising steadily and has not reached asymptotic steady-state. Additional thermocouple measurements were made on the vertical external faces of the array, and gave temperatures similar to the base and top, confirming the uniformity of the array temperature distribution.

Scattering characteristics (return loss and gain) of the entire amplifier array, Fig. 1, were studied for different thermal regimes by conducting an experiment in which a horn antenna was used to feed the array at both the input and output. The 5 × 5 patch array was placed within the center of the horn so that the ground plane of the array was in contact with the aperture of the horn. Dimensions for patch and slot antennas, substrate thickness, dielectric permittivity of the substrate, and other geometrical and material parameters of the amplifier array are given in [40]. Figs. 11 and 12 demonstrate a small-signal gain (S_{21}) and return loss (S_{11}) of the X-band amplifier array at different temperature levels, corresponding to ambient temperature at turn-on (solid line) and ∼25 K temperature rise of the aluminum framework at turn-off (dashed line).

It can be seen that the increase in temperature results in the change (decrease) of the small-signal gain by up to approximately 1 dB. Measured scattering characteristics S_{22} and S_{12} demonstrated a good isolation of the

input and output of the array at different temperature levels. (Note that in this design, Fig. 1, the input is at port 1 and the output is at port 2.)

VIII. Simulation Results

Fig. 13 shows the results of a coupled EM-electro-thermal, single-tone HB simulation of the spatial power combining array. This figure represents the first global simulation of such a structure. The figure illustrates the impact of thermal effects on total system output voltage waveform at the output waveguide.

The calculated response is sensitive to the thermal boundary conditions employed in describing the MMIC array. These are dependent on surface emissivity which is not a well specified parameter. Simulations show that transient rise time to steady-state, and the steady-state temperature achieved, are both highly sensitive to the value of surface emissivity and to the resulting ratio of radiative to convective losses.

This is illustrated in the thermal simulation of Fig. 14 which shows calculated transient response from turn on of the aluminum framework dissipating 20 W.

The calculation assumed heat loss purely by natural convection and radiation, with no heatsink mounting. As emissivity is neither uniform nor well known, three different average values were assumed: $\epsilon = 0.1$ (corresponding to commercial aluminum sheet or rough plate); $\epsilon = 0.3$ (corresponding to heavily oxidized aluminum); and $\epsilon = 1.0$ (corresponding to a matt black surface). To estimate the surface heat flux coefficient, T^4 grey-body radiation from all surfaces was assumed, in combination with an approximation to laminar convection over flat plates.

Fig. 14 predicts that temperature rises will be independent of emissivity for the first $\sim$30 minutes, rising to $\sim$25 K above ambient (initial) temperature. This figure is seen to be in excellent agreement with the measured temperature rise from turn-on of the X-band array, as described in Sec. VII-A, above. From this point on, both rise time to steady-state and corresponding steady-state temperature are seen to be highly dependent on average surface emissivity, as illustrated in Table 1.

Because of the high thermal conductivity of aluminum, the temperature variation across the entire aluminum framework is measured to be less than $\sim$5 K at the $\sim$30 minute temperature rise of $\sim$25 K. To contrast with the temperature uniformity of this 'tray/card' architecture, simulations and measurements are now presented for a passive grid array, of the general form illustrated in Fig. 2 [49]. The passive array considered consisted of a 10×10 array of resistors mounted on an FR-4 substrate, 5×5 cm^2. A Thermacam image of this array, dissipating 2 W, and essentially free-standing in a vertical plane, with the bottom edge at an angle of $45°$ to the horizontal, is illustrated in Fig. 15. The array is again cooled totally by radiation and convection with no heatsink mounting.

Because of the low thermal conductivity of the FR-4 substrate temperature variation amounts to $\sim$50 K across the whole array, and natural convection is seen to have a major impact on the measured temperature profile, causing a marked asymmetry of the temperature contours. Measured and simulated temperature rises from turn-on for this system are illustrated in Fig. 16, along with results of a corresponding simulation assuming AlN substrate.

In contrast to the less than 1 dB decrease in forward gain, S_{21}, observed for the global S-parameter measurements described in Sec. VII-A, measurements for a 38 GHz 3-stage balanced amplifier MMIC described by the authors previously [12], showed a $\sim$4 dB decrease in forward gain for a $\sim$30 K rise in active channel temperature. (Note that the indicated temperatures of 60 C and 70 C in Fig. 8 of [12] represent a typographical error, and the measured temperature range was actually 40 C to 70 C.) Taking this more sensitive temperature dependence for illustrative purposes, Fig. 17 shows extrapolated forward gain over a 10×10 MMIC array on FR-4 substrate. This figure illustrates $\sim$5 dB variation in S_{21} implying reduced beam integrity, power added efficiency (PAE) and stability, due to the MMIC base temperature variation across the array.

IX. Discussion

The coupled EM-electro-thermal model has been described and partially validated by comparison against experiment for two spatial power combining architectures illustrating electro-thermal effects. Some electro-thermal issues for spatial power combiner operation and modeling are now outlined.

A. Electro-thermal physics

Measurements have demonstrated temperature dependence of forward gain in a MMIC amplifier, S_{21}, decreasing up to $\sim$4 dB for a $\sim$30 K rise in temperature, depending on the nature of the amplifier [12]. Such a temperature effect on amplifier performance has been demonstrated here to have an $\sim$1 dB impact on global S-parameters for a 'tray/card' MMIC array (utilizing

different, 2-stage, MMIC amplifiers).

Simulations have indicated that without active cooling, temperature rises of spatial power combining arrays can be much larger than ∼30 K, depending crucially on factors like surface emissivity. Impact of temperature rise on global gain of such amplifiers could be significant. Transient temperature variation, either at turn-on or under pulsed operation, could then be important for large structures with a high heat capacity. Rise time to steady-state, and steady-state operating temperatures in such systems are greatly dependent on the corresponding surface flux boundary condition.

Spatial temperature non uniformity can also be an issue in MMIC arrays, though this is largely determined by the magnitude of the thermal conductivity of the substrate. High conductivity substrates, such as Al or AlN, give rise to small variation between MMIC base temperatures. However, such substrates can be bulky, heavy, fragile or expensive. Low cost, robust substrates, compatible with conventional electronic system technology can give large temperature non uniformity effects, due to low thermal conductivities, potentially impacting beam formation, and giving a dependence on device orientation due to surface convection [49].

Temperature rises of power combining systems are ultimately determined by surface flux losses or heat sinking. Whilst unwanted thermal effects can always be ameliorated by sufficient active cooling, such cooling imposes penalties in terms of a power overhead and reduced efficiency, and in size and weight of power combining systems. Where such considerations are important, the modeling tools described here can be expected to help in optimization of thermal design. In such global design, substrate conductivity, diffusivity, specific heat and device volume are key issues.

At MMIC level, all the standard considerations in thermal design apply. Time constants and steady-state temperature in the vicinity of the device channel are sensitive to the volume of the active region, the geometry of the MMIC die, and to detailed structure like surface metallization, air bridges, vias and base metallization.

Electro-thermal interactions can be exhibited as: hot spot formation, thermal runaway and burn-out; heating effects on reduced mobility and forward gain; thermal intermodulation distortion and spectral regrowth; parasitic thermal voltages at metal 1-metal 2 contacts; thermal feedback, input-output coupling and electro-thermal oscillations.

Although MMIC design and global power combiner structure can be largely decoupled, the modeling tools described here allow individual design at both ends of this spectrum, as well as allowing global simulation of the whole structure with accurately generated time constants from device channel to MMIC array. This allows, in principle, study of any coupling effects between subsystems with differing thermal time constants, that might arise as a result of system nonlinearity, *e.g.*, thermal intermodulation distortion. An investigation of thermally induced memory effects, and how they might interact with electrical terminations of similar time constants will be presented elsewhere. Preliminary studies have been presented in [50], [51]. At system level, electro-thermal interactions can potentially affect reliability, efficiency, beam formation and nonlinear distortion.

B. Modeling issues

A number of electro-thermal modeling issues are raised by the simulation of whole spatial power combining systems:

(i) Heat flow must be described in a fully 3-dimensional fashion. 2-dimensional simulations have been shown to be inadequate [52], [53]. CAD timescale electrical device descriptions can be (quasi-)2-dimensional, *i.e.*, 3-dimensional though ignoring 'end effects,' but must be properly coupled to a 3-dimensional heat flow model. The method described in this paper avoids approximation of thermal boundary conditions at the limits of the (much smaller) electrical simulation domain.

(ii) Non linearity of the heat diffusion equation (temperature dependent material parameters), as well as nonlinearity of surface fluxes, impact steady-state temperature and time constants. External boundary conditions due to convection and radiation must be fully treated in large area systems.

(iii) Accurate calculations of thermal response require full treatment of device structural detail from MMIC to MMIC array level.

(iv) Thermal models must be compact to allow CAD timescale coupled electro-thermal solution.

(v) At the circuit level there is an intrinsic problem due to the huge range of time constants varying from ∼100 GHz signals to ∼10,000 s transients.

(vi) Circuit level simulations must also represent the true nature of complex signal formats such as CDMA.

(vii) The electro-thermal model must treat accurately multi-tone spectra and adjacent channel power ratio (ACPR), with asymmetry due to memory and hystere-

sis effects (due to trapping, thermal intermodulation and bias impedance).

X. Conclusion

The first CAD tool capable of global, coupled EM-electro-thermal simulation of a whole microwave subsystem has been outlined, and illustrated for the first time by simulation of a whole spatial power combining array. Parallel developments in thermal and EM measurement have allowed partial validation of the model. Electro-thermal issues for the operation, and the modeling, of spatial power combining systems have been indicated. The global CAD tools and characterization techniques described here will allow design optimization, and study of fundamental physics, in the operation of spatial power combiners for use as high power sources at millimeter wavelengths.

XI. Acknowledgement

References

[1] W. Batty, C. E. Christoffersen, A. B. Yakovlev, J. F. Whitaker, M. Ozkar, S. Ortiz, A. Mortazawi, R. Reano, K. Yang, L. P. B. Katehi, C. M. Snowden and M. B. Steer, "Global coupled EM-electrical-thermal simulation and experimental validation for a spatial power combining MMIC array," *IEEE MTT-S Internat. Microwave Symp. Dig.*, Paper IF-TH-49, Vol. 3, pp. 2177–2180, June 2002.

[2] S. Ortiz and A. Mortazawi, "A perpendicularly-fed patch array for quasi-optical power combining," *1999 MTT-S IEEE Int. Microwave Symp. Dig.*, pp. 667–670, June 1999.

[3] C. E. Christoffersen, U. A. Mughal, M. B. Steer, "Object oriented microwave circuit simulation," *Int. J. RF and Microwave CAE*, Vol. 10, No. 3, pp. 164–182, 2000.

[4] M. B. Steer, J. F. Harvey, J. W. Mink, M. N. Abdulla, C. E. Christoffersen, H. M. Gutierrez, P. L. Heron, C. W. Hicks, A. I. Khalil, U. A. Mughal, S. Nakazawa, T. W. Nuteson, J. Patwardhan, S. G. Skaggs, M. A. Summers, S. Wang and A. B. Yakovlev, "Global modeling of spatially distributed microwave and millimeter-wave systems," *IEEE Trans. Microwave Theory Tech.*, Vol. 47, pp. 830–839, 1999.

[5] C. E. Christoffersen and M. B. Steer, "Implementation of the local reference concept for spatially distributed circuits," *Int. J. of RF and Microwave Computer-Aided Eng.*, Vol. 9, No. 5, pp. 376–384, 1999.

[6] M. B. Steer and C. E. Christoffersen , "Generalized circuit formulation for the transient simulation of circuits using wavelet, convolution and time-marching techniques," *Proc. of the 15th European Conference on Circuit Theory and Design*, pp. 205–208, August 2001.

[7] C. E. Christoffersen, M. B. Steer and M. A. Summers, "Harmonic balance analysis for systems with circuit-field interactions," *IEEE Int. Microwave Symp. Dig.*, pp. 1131-1134, June 1998.

[8] C. E. Christoffersen, M. Ozkar, M. B. Steer, M. G. Case and M. Rodwell, "State-variable-based transient analysis using convolution," *IEEE Trans. Microwave Theory Tech.*, Vol. 47, No. 6, pp. 882–889, 1999.

[9] C. E. Christoffersen and M. B. Steer, "State-variable-based transient circuit simulation using wavelets," *IEEE Microwave Wireless Components Lett.*, Vol. 11, pp. 16–23, Apr. 2001.

[10] C. E. Christoffersen, *Global modeling of nonlinear microwave circuits*, Ph.D. Dissertation, North Carolina State University, Dec. 2000.

[11] fREEDA^{TM} software online: http://www.freeda.org.

[12] W. Batty, A. J. Panks, R. G. Johnson and C. M. Snowden, "Electro-thermal modeling and measurement for spatial power combining at millimeter wavelengths," *IEEE Trans. Microwave Theory Tech.*, Vol. 47, No. 12, pp. 2574–2585, 1999.

[13] W. Batty, A. J. Panks, R. G. Johnson and C. M. Snowden, "Electro-thermal modeling of monolithic and hybrid microwave and millimeter wave IC's," *VLSI Design*, Vol. 10, No. 4, pp. 355–389, 2000.

[14] W. Batty, C. E. Christoffersen, A. J. Panks, S. David, C. M. Snowden and M. B. Steer, "Electro-thermal CAD of power devices and circuits with fully physical time-dependent compact thermal modeling of complex nonlinear 3-d systems," *IEEE Trans. Comp. Packag. Technol.*, Vol. 24, No. 4, pp. 566–590, Dec. 2001.

[15] W. Batty and C. M. Snowden, "Electro-thermal device and circuit simulation with thermal nonlinearity due to temperature dependent diffusivity," *Electron. Lett.*, Vol. 36, pp. 1966–1968, 2000.

[16] K. Krabbenhoft and L. Damkilde, "Comment: Electro-thermal device and circuit simulation with thermal nonlinearity due to temperature dependent diffusivity," *Electron. Lett.*, Vol. 37, pp. 1481– 1482, 2001.

[17] W. Batty, S. David and C. M. Snowden, "Reply to Comment on 'Electro-Thermal Device and Circuit Simulation with Thermal Non Linearity due to Temperature Dependent Diffusivity'," *Electron. Lett.*, Vol. 37, pp. 1482–1483, 2001.

[18] W. Batty, S. David, A. J. Panks, R. G. Johnson and C. M. Snowden, "Series acceleration of a compact thermal model and fast nonlinear optimization of electrothermal device design," *Proc. 7th Internat. Workshop on Thermal Investigations of ICs and Systems (THERMINIC 2001)*, Paris, pp. 11–16, Sept. 2001.

[19] W. Batty, C. E. Christoffersen, C. M. Snowden and M. B. Steer, "Fully physical coupled electro-thermal modeling of power devices and circuits," *Proc. 13th Workshop Physical Simulation of Semicond. Dev. (PSSD)*, Session 3, Ilkely, UK, March 2002.

[20] W. Batty, A. J. Panks, C. E. Christoffersen, S. David, R. G. Johnson, C. M. Snowden and M. B. Steer, "Fully analytical compact thermal model of complex electronic power devices and packages in coupled electrothermal CAD," *Proc. 7th Internat. Workshop on Thermal Investigations of ICs and Systems (THERMINIC 2001)*, Paris, pp. 99–102, Sept. 2001.

[21] H. Stehfest, "Algorithm 368 Numerical inversion of Laplace transforms [D5]," *Comm. ACM*, Vol. 13, No. 1, pp. 47–49 and 624, 1970.

[22] P. Satravaha and S. Zhu, "An application of the LTDRM to transient diffusion problems with nonlinear material properties and nonlinear boundary conditions," *Appl. Math. Comp.*, Vol. 87, No. 2–3, pp. 127–160, 1997.

[23] A. Csendes, V. Szekely, M. Rencz, "An efficient thermal simulation tool for ICs, microsystem elements and MCMs: the μS-THERMANAL," *Microelectron. J.*, Vol. 29, 241–255, 1998.

[24] V. Szekely, A. Pahi and M. Rencz, "SUNRED, a new field solving approach," *Proc. Symp. Design, Test and Microfab. of MEMS and MOEMS*, SPIE Vol. 3680, No. 1, pp. 278-288, 1999.

[25] V. Szekely, "THERMODEL: a tool for compact dynamic thermal model generation," *Microelectron. J.*, Vol. 29, pp. 257–267, 1998.

[26] A. R. Hefner and D. L. Blackburn, "Simulating the dynamic electrothermal behavior of power electronics and circuits," *IEEE Trans. Power Electron. Dev.*, Vol. 8, No. 4, pp. 376–385, 1993.

[27] A. R. Hefner and D. L. Blackburn, "Thermal component models for electrothermal network simulation," *IEEE Trans. Comp., Packag., and Manufact. Technol. – Part A*, Vol. 17, No. 3, pp. 413–424, 1994.

[28] P. W. Webb, "Thermal design of gallium arsenide MESFETs for microwave power amplifiers," *IEE Proc.-Circuits Devices Syst.*, Vol. 144, No. 1, pp. 45–50, 1997.

[29] K. S. Kundert, J. K. White and A. Sangiovanni-Vincentelli, *Steady-state Methods for Simulating Analog and Microwave Circuits*, Kluwer Academic Publishers, 1990.

[30] V. Borich, J. East and G. Haddad, "An efficient Fourier transform algorithm for multitone harmonic balance," *IEEE Trans. Microwave Theory Tech.,*, Vol. 47, No. 2, pp. 182–188, Feb. 1999.

[31] C. M. Snowden and R. R. Pantoja, "Quasi-two-dimensional MESFET simulations for CAD," *IEEE Trans. Electron Dev.*, Vol. 36, pp. 1564–1574, 1989.

[32] C. G. Morton, J. S. Atherton, C. M. Snowden, R. D. Pollard and M. J. Howes, "A large-signal physical HEMT model," *IEEE MTT-S Internat. Microwave Symp. Dig.*, pp. 1759–1762, 1996.

[33] R. G. Johnson, C. M. Snowden and R. D. Pollard, "A physics-based electro-thermal model for microwave and millimeter wave HEMTs," *IEEE MTT-S Internat. Microwave Symp. Dig.*, Vol. 3, Paper TH3E-6, pp. 1485–1488, 1997.

[34] L. Albasha, R. G. Johnson, C. M. Snowden and R. D. Pollard, "An investigation of breakdown in power HEMTs and MESFETs utilizing an advanced temperature-dependent physical model," *Proc. IEEE 24th Internat. Symp. Compound Semiconductors*, pp. 471–474, San Diego, 1997.

[35] W. Batty, C. E. Christoffersen, C. M. Snowden and M. B. Steer, "Coupled electro-thermal physical device simulation in global microwave circuit modeling," *IEEE MTT-S Internat. Microwave Symp.*, Workshop WSG: GHz and THz Solid State Device Simulation, June 2002.

[36] Z. Yu, R. W. Dutton, B. Troyanovsky and J. Sato-Iwanaga, "Large signal analysis of RF circuits in device simulation," *IEICE Trans. Electron.*, Vol. E82-C, No. 6, pp. 908–916, 1999.

[37] A. J. Panks, W. Batty, S. David, R. G. Johnson and C. M. Snowden, "Fully physical electro-thermal CAD for power FET optimization by non uniform finger spacing," *Proc. 9th European GaAs and other semiconductors Application Symp. (GAAS 2001)*, pp. 191–194, London 2001.

[38] C. M. Snowden, "Electrothermal transistor models for large-signal design," *IEEE MTT-S Internat. Microwave Symp.*, Workshop WFG: Developments in Time-Domain Methods for Non-Linear CAD, 1998.

[39] Y. Xuan and C. M. Snowden, "A new frequency domain physical device simulation technique," *IEEE Internat. Symp. Circ. Syst.*, Vol. 1, pp. 93–96, 1990.

[40] A. B. Yakovlev, S. Ortiz, M. Ozkar, A. Mortazawi, and M. B. Steer, "A waveguide-based aperture-coupled patch amplifier array — full-wave system analysis and experimental validation," *IEEE Trans. Microwave Theory Tech.,* Vol. 48, pp. 2692–2699, Dec. 2000.

[41] A. B. Yakovlev, S. Ortiz, M. Ozkar, A. Mortazawi, and M. B. Steer, "Electric dyadic Green's functions for modeling resonance and coupling effects in waveguide-based aperture-coupled patch arrays," *Applied Computational Electromagnetics Society (ACES) J.*, July 2002.

[42] H. Patzelt and F. Arndt, "Double-plane steps in rectangular waveguides and their application for transformers, irises, and filters," *IEEE Trans. Microwave Theory Tech.*, Vol. 30, pp. 771–776, May 1982.

[43] W. T. Beyene and J. E. Schutt-Ainee, "Efficient transient simulation of high-speed interconnects characterized by sampled data", *IEEE Trans. on Components, Packaging and Manufacturing Techn. – Part B*, Vol. 21, No. 1, pp. 105-114, Feb. 1998.

[44] R. Achar and M. S. Nakhla, "Simulation of high-speed interconnects," *Proc. IEEE*, Vol. 89, No. 5, pp. 693–728, May 2001.

[45] K. Yang, G. David, S. Robertson, J. F. Whitaker, and L. P. B. Katehi, "Electro-optic mapping of near-field distributions in integrated microwave circuits," *IEEE Trans. Microwave Theory Tech.,* Vol. 46, pp. 2338–2343, Dec. 1998.

[46] K. Yang, T. Marshall, M. Forman, J. Hubert, L. Mirth, Z. Popovic, L. P. B. Katehi, and J. F. Whitaker, "Active-amplifier-array diagnostics using high-resolution electro-optic field mapping," *IEEE Trans. Microwave Theory Tech.,* Vol. 49, pp. 849–857, May 2001.

[47] K. Yang, L. P. B. Katehi, and J. F. Whitaker, "Electric-field mapping system using an optical-fiber-based electro-optic probe," *IEEE Microwave Wireless Comp. Lett.,* Vol. 11, pp. 164–166, Apr. 2001.

[48] R. M. Reano, K. Yang, J. F. Whitaker, and L. P. B. Katehi, "Simultaneous measurements of electric and thermal fields utilizing an electrooptic semiconductor probe," *IEEE Trans. Microwave Theory Tech.*, Vol. 49, pp. 2523–2531, Dec. 2001.

[49] W. Batty, A. J. Panks, S. David, R. G. Johnson and C. M. Snowden, "Electro-thermal modeling and measurement of thermal time constants and natural convection in MMIC grid arrays for spatial power combining," *IEEE MTT-S Internat. Microwave Symp. Dig.*, Vol. 3, pp. 1937–1940, 2000.

[50] S. David, W. Batty, A. J. Panks, R. G. Johnson and C. M. Snowden, "Thermal transients in microwave active devices and their influence on intermodulation distortion," *IEEE MTT-S Internat. Microwave Symp. Dig.*, Vol. 1, pp. 431–434, 2001.

[51] S. David, W. Batty, A. J. Panks, R. G. Johnson and C. M. Snowden, "Simulation of thermally induced intermodulation distortion," *Proc. 13th Workshop on Physical Simulation of Semiconductor Devices*, Ilkley, UK, pp. March 2002.

[52] P. W. Webb, "Thermal modeling of power gallium arsenide microwave integrated circuits," *IEEE Trans. Electron Dev.*, Vol. 40, No. 5, pp. 867–877, 1993.

[53] V. d'Alessandro and N. Rinaldi, "A critical review of thermal models for electro-thermal simulation," *Sol.-Stat. Electron.*, Vol. 46, pp. 487–496, 2002.

TABLE I

TABLE 1: EFFECT OF AVERAGE SURFACE EMISSIVITY, ϵ, ON: RISE TIME TO 90% OF STEADY-STATE TEMPERATURE, τ_{90}; MAGNITUDE OF STEADY-STATE TEMPERATURE, T_{steady}; AND CORRESPONDING POWER DISSIPATION BY CONVECTION (AS OPPOSED TO RADIATION) P_{conv}.

ϵ	τ_{90} (hours)	T_{steady} (K)	P_{conv} (W)
0.1	7	413	15
0.3	4	383	10
1.0	1	346	5
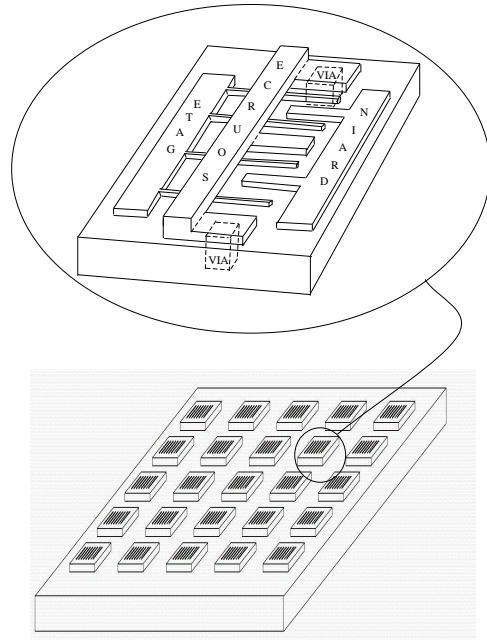
Fig. 2. Schematic (not to scale) of a power FET grid array representative of one form of spatial power combiner architecture.
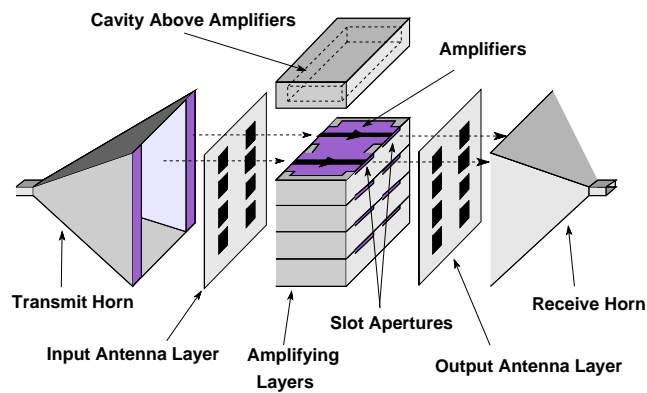
Fig. 1. X-band 'tray/card' MMIC array spatial power combiner used for global EM-electro-thermal simulation and experimental validation.
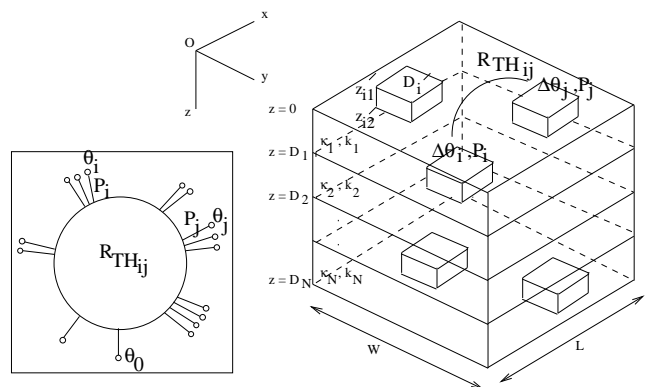
Fig. 3. N-level multilayer with arbitrarily distributed volume sources for fully analytical construction of thermal impedance matrix $R_{TH_{ij}}(s)$. Inset: N-port described by generalized multiport thermal Z-parameters, $R_{TH_{ij}}(s)$.
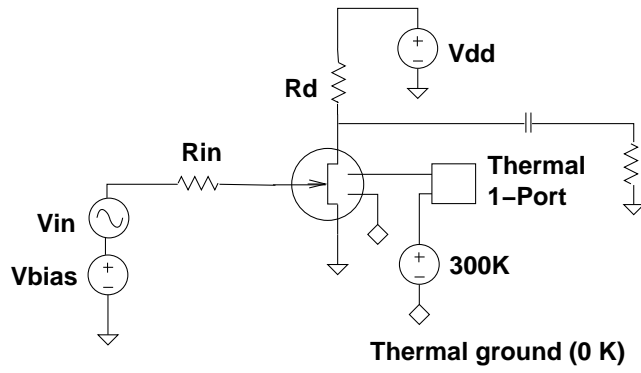
Fig. 4. Electro-thermal circuit for illustration of DC and transient implementation of the Leeds Physical Model in fREEDA^{TM}.
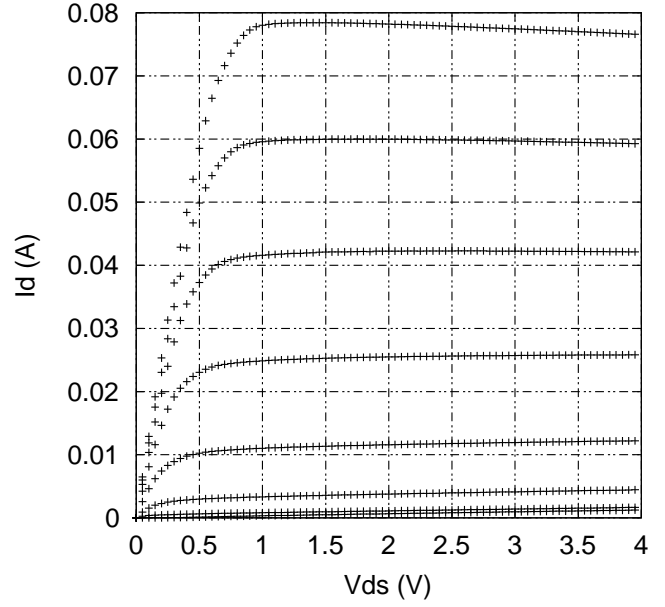
Fig. 6. Fully coupled electro-thermal DC simulation for a power HEMT based on the LPM in fREEDA^{TM}.
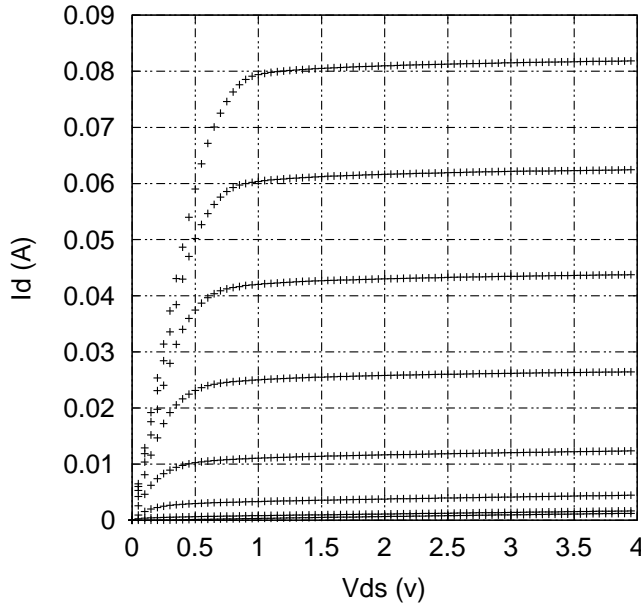
Fig. 5. Isothermal DC simulation for a power HEMT based on the LPM in fREEDA^{TM}.
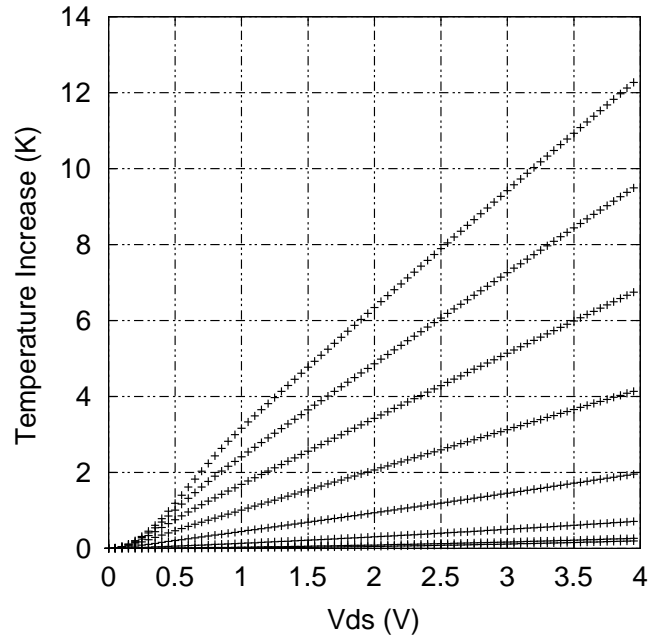
Fig. 7. Temperature rise in the device channel of a power HEMT as a function of applied bias, by coupled electro-thermal DC simulation based on the LPM in fREEDA^{TM}.
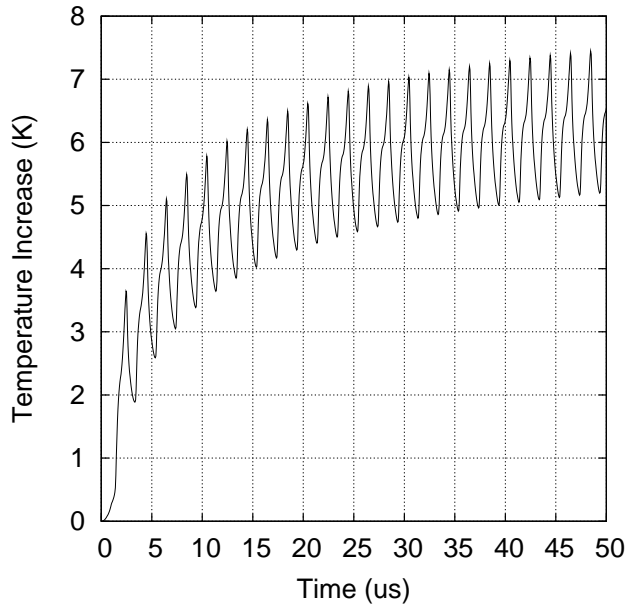
Fig. 8. Fully coupled electro-thermal RF simulation, showing temperature rise as a function of time t in the active device channel of a power HEMT, based on the LPM in fREEDA^{TM}.
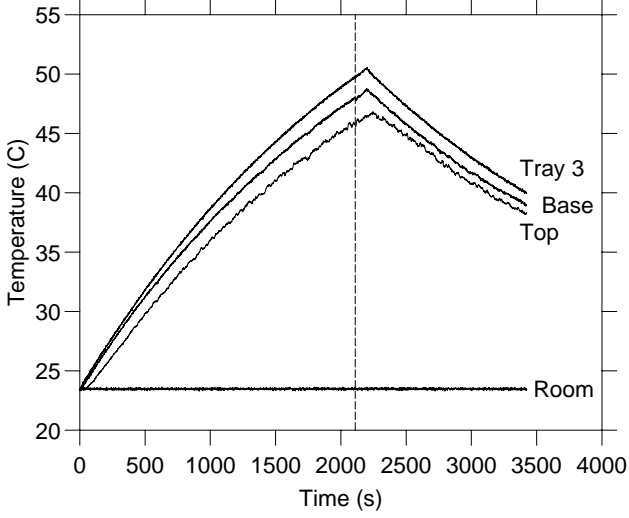
Fig. 10. Thermocouple measurements of temperature rise in X-band array at turn on. V = 6.001 V, I = 3.285 A, power = 19.7 W.
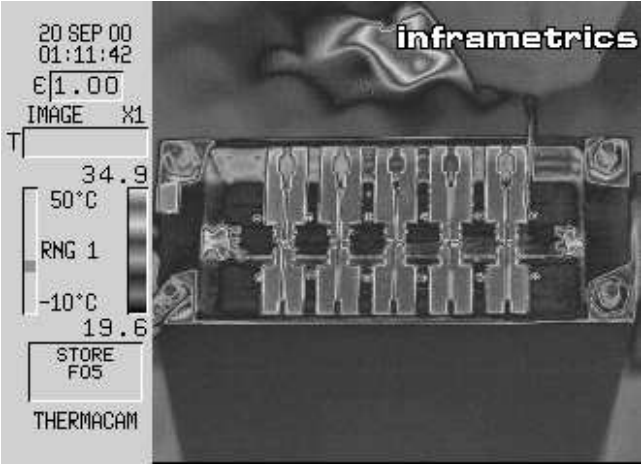
Fig. 9. Infrared thermal image of a lateral cross-section of the X-band 'tray/card' MMIC array, showing 5 MMIC die.
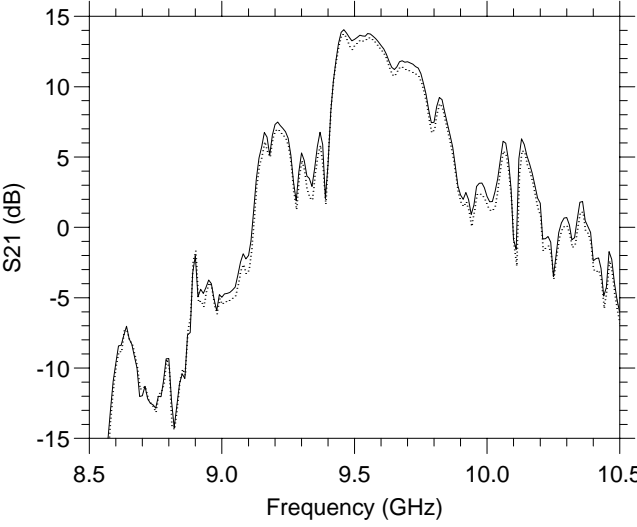
Fig. 11. Measured global S-parameters, S_{21}, for the X-band array as a function of frequency and temperature. Initial ambient temperature: solid line. Maximum temperature: dashed line.
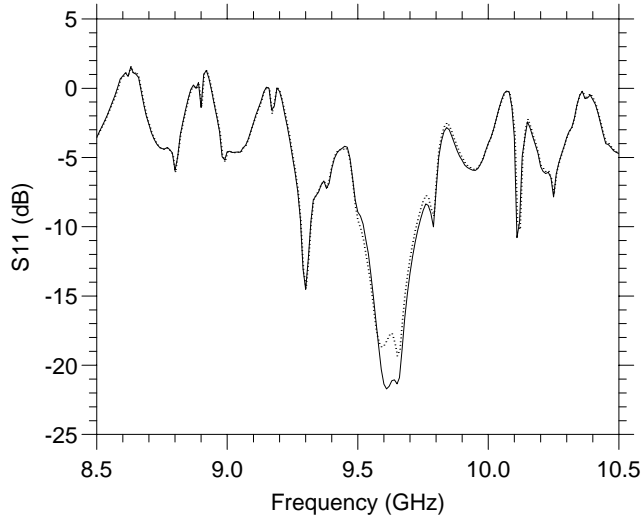
Fig. 12.   Measured global S-parameters, S_{11}, for the X-band array as a function of frequency and temperature. Initial ambient temperature: solid line. Maximum temperature: dashed line.
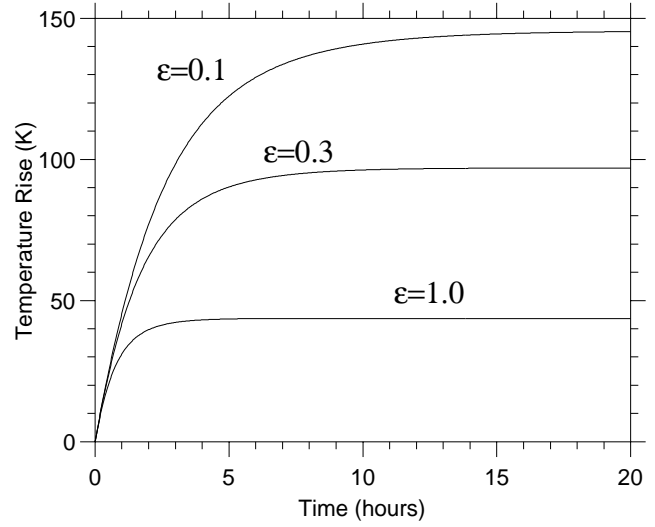

Fig. 14.   Temperature rise against time from turn-on, for the X-band array dissipating 20 W, as a function of average surface emissivity.
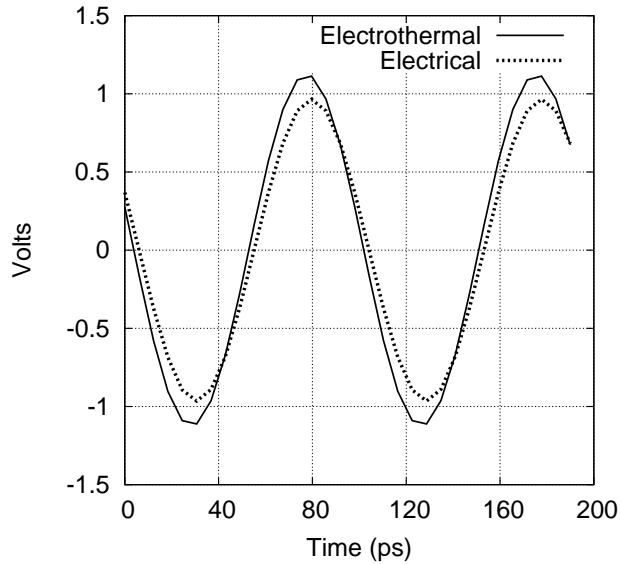

Fig. 13.   Coupled EM-electro-thermal, single-tone HB simulation of the X-band spatial power combining MMIC array, illustrating thermal effects on total system output.
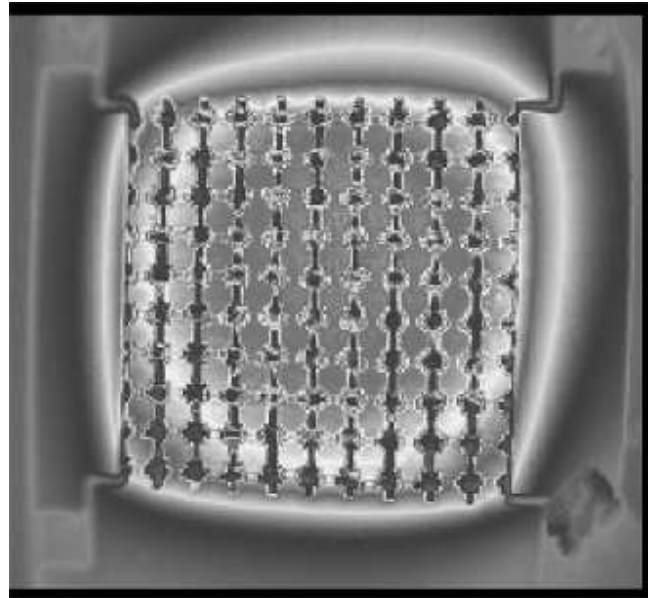

Fig. 15.   Inframetrics Thermacam measurement of vertically mounted 10×10 passive array (5×5 cm^2) mounted at an angle of $45°$. Convection means that beam profile can be distorted by choice of orientation.
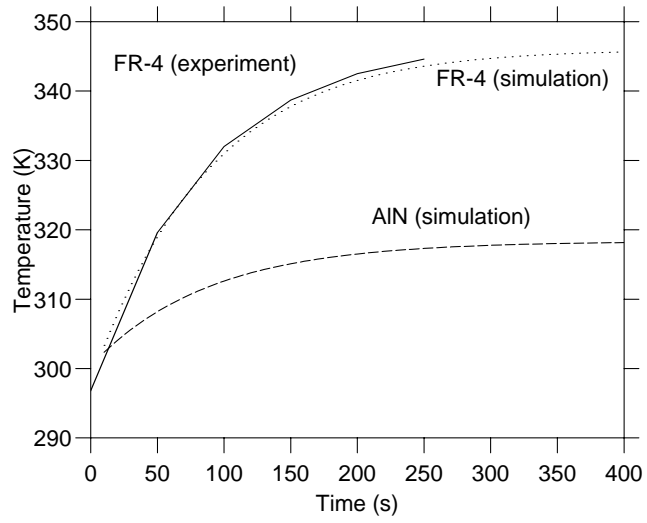
Fig. 16. Comparison of measured and simulated temperature rise, as a function of time from turn-on, at the center of the FR-4 10×10 passive array dissipating 2 W. Also shown, calculated temperature rise assuming an AlN substrate.
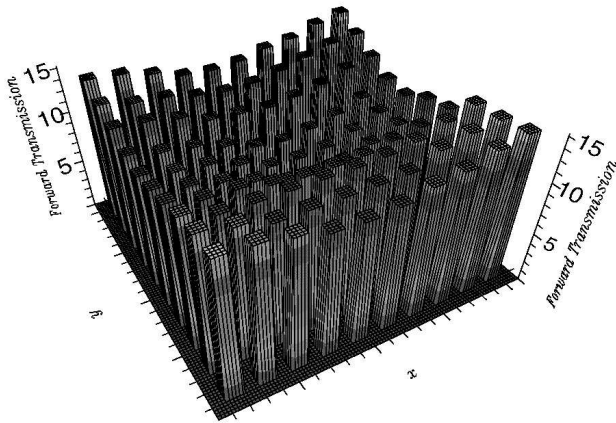

Fig. 17. Extrapolated S_{21} (in dB) across a 10×10 MMIC array. 5 dB variation implies reduced beam integrity, PAE and stability, due to MMIC base temperature variation across the array.